actuators

MDPI

Article

Preparation of Ionic Polymer–Metal Composites Using Copper Electrodes via Magnetron Sputtering

Hui Li [1,2,3,*], Zhifeng Wang [1,2,3,4,*], Jinping Li [1], Chunmeng Wu [2,4], Minghuan Guo [2,3,4], Huibin Zhu [2,3,4], Jing Li [1,2,3] and Cheng Zhang [1,2,3]

1 College of Energy and Power Engineering, Lanzhou University of Technology, Lanzhou 730050, China
2 Institute of Electrical Engineering, Chinese Academy of Sciences, Beijing 100190, China
3 Beijing Engineering Research Center of Solar Thermal Power, Beijing 100190, China
4 University of Chinese Academy of Sciences, Beijing 100049, China
* Correspondence: lihui2152@mail.iee.ac.cn (H.L.); zhifeng@vip.sina.com (Z.W.)

Abstract: The effective treatment of the surface electrode is the core technology of an ionic polymer–metal composite (IPMC), and its preparation significantly affects the driving performance of the IPMC. Copper, which is inexpensive and has excellent electrical conductivity, was selected as the surface electrode material, and copper electrode IPMCs (Cu-IPMCs) were prepared via magnetron sputtering. Orthogonal experiments were performed to optimize the parameters of the preparation process. The indices of the deformation angle and surface resistance were used, and the sample electrodes' surface morphology and elemental content were analyzed. The results showed that sputtering pressure was the major factor affecting two indices. The Cu-IPMC, prepared at a sputtering pressure of 0.9 Pa, sputtering time of 35 min, argon flow rate of 30 sccm, and sputtering power of 150 W, had a more minor surface resistance and a larger deformation angle under continuous direct current boosting. It required a sputtering time of 1.2 h, which was more than 10 times shorter than its chemically plated counterpart. It exhibited surface resistance in the 2–3 Ω/cm range, which was 23 times smaller than chemically plated platinum.

Keywords: magnetron sputtering; orthogonal experiment; Cu-IPMC; surface resistance; flexible surface

Citation: Li, H.; Wang, Z.; Li, J.; Wu, C.; Guo, M.; Zhu, H.; Li, J.; Zhang, C. Preparation of Ionic Polymer–Metal Composites Using Copper Electrodes via Magnetron Sputtering. *Actuators* **2024**, *13*, 503. https://doi.org/10.3390/act13120503

Academic Editor: Shuxiang Dong

Received: 23 October 2024
Revised: 1 December 2024
Accepted: 5 December 2024
Published: 7 December 2024

1. Introduction

Smart materials have promising applications in different fields of modern industry, such as soft robotics [1–3], biomedicine [4,5], actuators, sensors [6,7], and microelectromechanical systems (MEMS) [8,9], owing to their unique properties of sensing external stimuli and their actuation capabilities. Ionic Polymer–metal Composite (IPMC) is one type of smart material that has three layers and where the middle layer is an ion-exchange membrane, while the upper and lower layers are layers of metal electrodes or non-metallic electrodes with a specific thickness, deposited via physical or chemical methods [10–12]. It can undergo significant size and shape changes under low-voltage excitation [13,14] and can be used to fabricate displacement actuators and make them lightweight and miniaturized [15,16]. The IPMC contains anionic ends dominated by a fluorocarbon backbone, hydrated cations dominated by sodium ions, and free water molecules capable of bending under an applied electric field [17–20]. When a voltage is applied to the two electrodes of the IPMC, the cations in the matrix membrane drag the water molecules to form hydrated cations and migrate together to the cathode under the stimulation of the voltage. Due to the effect of migration, there is a difference in the distribution of the hydrated cations on the anode side and the cathode side, resulting in a different pressure within the substrate membrane, which leads to the bending and deformation of the IPMC. In addition, the deformation mechanism of IPMCs involves electrochemical reactions. When

hydrated cations migrate, charge transfer occurs, which causes current flow, leading to electrochemical responses [21,22].

IPMCs are typically fabricated by chemically plating platinum electrodes on both surfaces of an ion-exchange membrane [23]. Several studies on IPMCs have recently focused on electrode fabrication to improve driving performance. Electrodes with low resistance and chemical stability are guaranteed to enhance IPMC drive performance. Generally, the lower the surface electrode resistance of the IPMC, the stronger its driving ability [24]. To reduce the surface electrode resistance, L. N. Hao et al. doped multiwalled carbon nanotubes into the base membrane to prepare IPMCs with dimensions of 30 mm × 5 mm × 0.4 mm. The resistance of the entire length was 104.5 Ω, which was 48.9 Ω lower than that of traditional IPMCs [25]. Scientists used the material with the best electrical conductivity, Ag, for doping. For instance, Chung et al. chemically plated Ag onto the surface of an Ag-doped nanopowder-based film [26], which improved the driving performance to some extent; Fu et al. used magnetron sputtering for plating Ag onto a substrate film to prepare an Ag-IPMC for application in the real-time monitoring of human movement using wearable devices [6]; however, this method is primarily used for sensors and does not address performance testing related to actuators. The traditional Pt-IPMC has a relatively high surface resistance. Someone attempted to remedy this by doping with other electrodes. For instance, Kim et al. first coated Pd metal particles onto the substrate membrane as a buffer layer before chemically plating with Pt. The Pd metal particles of the metal electrode IPMC penetrated the Nafion polymer film up to a depth of 30 μm. Such an IPMC structure can form a bilayer capacitor [27,28]; however, it is difficult to accurately control the chemical process for the thickness of the two coatings. The magnetron sputtering coating process is simple; the preparation efficiency is high. Compared to silver, copper is very inexpensive and has excellent electrical conductivity. However, there is a gap in IPMC research on magnetron-sputtered copper electrodes, and the basic process flow and influencing factors are ambiguous. This study explored the magnetron sputtering method for preparing IPMCs by plating copper onto substrate films, and orthogonal experiments were performed to optimize the process parameters. The electrode surface topography, surface resistance, elemental content, and deformation angle of the Cu-IPMCs were analyzed, and the specimen with the best performance was determined. A Cu-IPMC prepared by magnetron sputtering exhibits a smoother surface and better surface reflectivity. The preparation process is simple, and the preparation time is significantly reduced, making it more suitable for mass production. Moreover, copper's electrical conductivity is second only to silver, and the price of copper targets is more than ten times cheaper than those of platinum and silver, making copper more cost-effective. Finally, we used optimization software to mathematically fit the deformation surface of IPMC, which allows us to determine the type of deformation surface. This is of significant importance for the preliminary exploration of flexible surface deformation concentrators.

2. Materials and Methods

2.1. Materials

The materials used in this study were Nafion117 film (DuPont, Wilmington, DE, USA), a copper target (High-purity copper, 99.9995%, Φ76.2 mm × 5 mm, Beijing Zhongnuo New Material Technology Co., Ltd., Beijing, China), Ar (99.99%, Beijing Lvyang Tiangang Technology Development Co., Ltd., Beijing, China), dilute hydrochloric acid (2 mol/L), and deionized water (Shenzhen Bida Environmental Protection Technology Co., Ltd., Shenzhen, China).

The experimental instruments mainly included dual-chamber high-vacuum magnetron sputtering thin-film deposition equipment (PVD500, Chinese Academy of Sciences Sky Technology Development Co., Ltd., Shenyang, China), laser displacement sensors (MS-LC100RS, Measurement range 65–135 mm, Shenzhen Opei Technology Co., Ltd., Shenzhen, China), an optical stage (600 mm × 600 mm × 13 mm, Wuhan Guangyu Trading Co., Ltd., Wuhan, China), a three-axis micro-adjustment stage (LD60-L, Dongguan Changan Shang

Pneumatic Hydraulic Co., Ltd., Dongguan, China), a triple-channel programmable DC power supply (GW Instek GPP-6030, Good Will Instrument Co., Ltd., Suzhou, China, a low-resistance tester (TH2512B, Changzhou Tonghui Electronics Co., Ltd., Changzhou, China), an electric heating furnace (Changde Beekman Biotechnology Co., Ltd., Changde, China), an electric sanding machine (#1200 sandpaper, Yiwu Xianger E-commerce Co., Ltd., Yiwu, China), scanning electron microscopy (SEM) testing equipment and energy-dispersive X-ray spectroscopy (EDS) testing equipment (Sigma, Carl Zeiss, Jena, Germany), and an ultrasonic cleaner (Beijing Lean Ronghua Equipment Co., Ltd., Beijing, China).

2.1.1. Pretreatment of the Substrate Membrane

The Nafion substrate membranes were pretreated before the magnetron sputtering process used to prepare the Cu-IPMCs. This ensured that each substrate membrane had the same water content and roughness. The preparation process is as follows: The two surfaces of the Nafion film were first sanded using an electric grinder to increase the surface roughness. The electric sander was used at 800 r/min. The machine's sanding head was fitted with #1200 abrasive paper, and the surface of the substrate film was sanded horizontally and vertically 50 times for 5 min on each side, for a total of 10 min for the two surfaces. This was followed by ultrasonic cleaning to remove sand and residue. Subsequently, the matrix membrane was boiled in a 2 mol/L dilute hydrochloric acid solution at 80 °C for 30 min to remove additives and ions from the matrix membrane. Finally, it was rinsed in deionized water, boiled at 80 °C for 30 min to remove the acid and to make it absorbent and swell, and then stored in deionized water. The pretreatment process for the substrate membrane is illustrated in Figure 1.

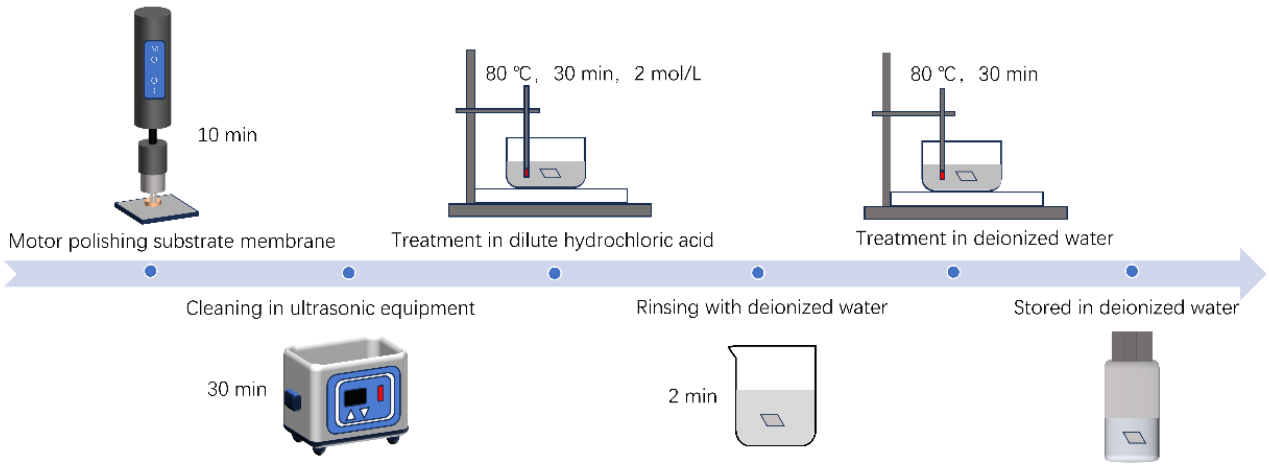

Figure 1. Pretreatment process for the substrate membrane.

2.1.2. Preparation of Cu-IPMCs via the Magnetron Sputtering Method

The preparation process is as follows: First, a high-purity copper target, which is the material used for preparing the IPMC electrodes, was installed in the magnetron sputtering equipment. The pretreated substrate film was placed in the feed chamber of the magnetron sputtering equipment. Subsequently, a high vacuum environment was maintained by vacuum pumps. Ar gas was passed through the sputtering chamber, and process parameters, such as the gas flow rate, target pressure, target power, and process time, were varied. After that, an automatic processing program was initiated to plate the copper electrodes onto the substrate film. Finally, the Cu-IPMC sample was removed at the end of the process, its shape was processed and assembled using copper metal sheets and copper conductors, and the assembled parts were subjected to subsequent testing. A schematic of the Cu-IPMC preparation via magnetron sputtering is shown in Figure 2.

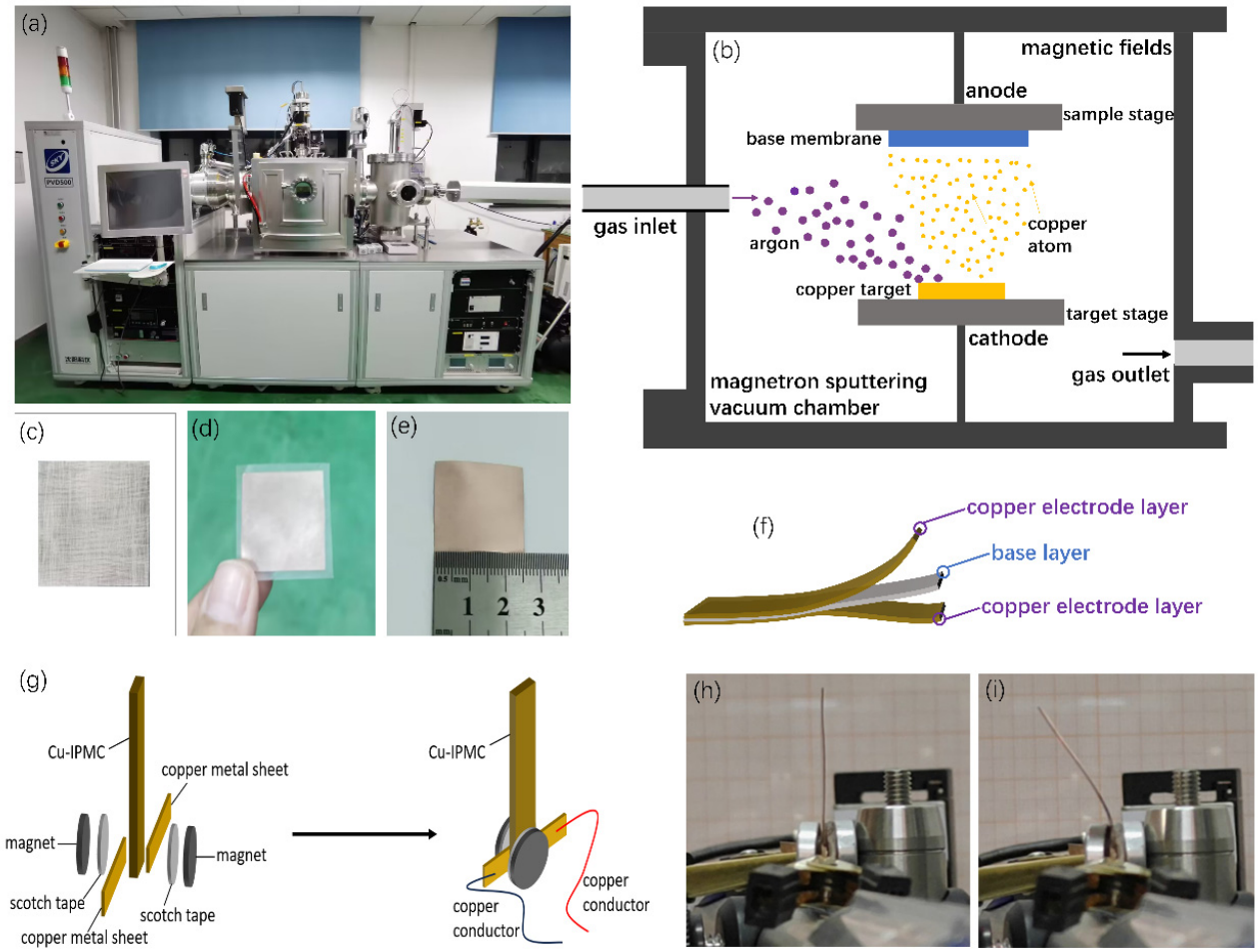

Figure 2. Images showing the (**a**) magnetron sputtering equipment, (**b**) sputtering deposition process, (**c**) polished Nafion117 sample, (**d**) Cu-IPMC uncut sample, (**e**) Cu-IPMC sample, (**f**) schematic of the Cu-IPMC "sandwich" structure, (**g**) strip-shaped Cu-IPMC assembly test structure, (**h**) strip-shaped Cu-IPMC without voltage, and (**i**) strip-shaped Cu-IPMC with voltage.

In magnetron sputtering equipment, a vacuum environment was maintained by a vacuum pump. The vacuum chamber was filled with the inert gas argon and, under high pressure, the Ar atoms ionized into Ar^+ and electrons, producing a plasma glow discharge. Electrons, while accelerating towards the substrate, were deflected by a magnetic field perpendicular to the electric field, confining them within a plasma region close to the target surface. Electrons, in the process of movement, constantly collided with the Ar atoms, ionizing a large number of Ar^+. Ar^+ was accelerated under the action of the electric field, impacting the target surface and releasing energy, resulting in the surface of the target atoms absorbing the kinetic energy of Ar^+. This caused the target atoms to break away from their original crystal lattice binding, and neutral target atoms escaped from the surface of the target material to fly to the substrate, where they were deposited to form a thin film [29].

2.2. Cu-IPMC Test Methods and Principles

An electrically excited response-driven test setup was used to measure the electromechanical drive performance of the Cu-IPMC, as shown in Figure 3. The electrically excited response-driven test rig consisted of an optical stage, a three-axis fine-tuning stage, a programmable power supply, a displacement test device (i.e., a laser displacement sensor), a transducer, and a sample fixture. Among these, the laser displacement sensor is primarily used to measure the change in the deformation displacement accurately when the Cu-IPMC

samples are deformed and to store the collected deformation displacement, voltage, current, and other related data in the computer using the data acquisition software.

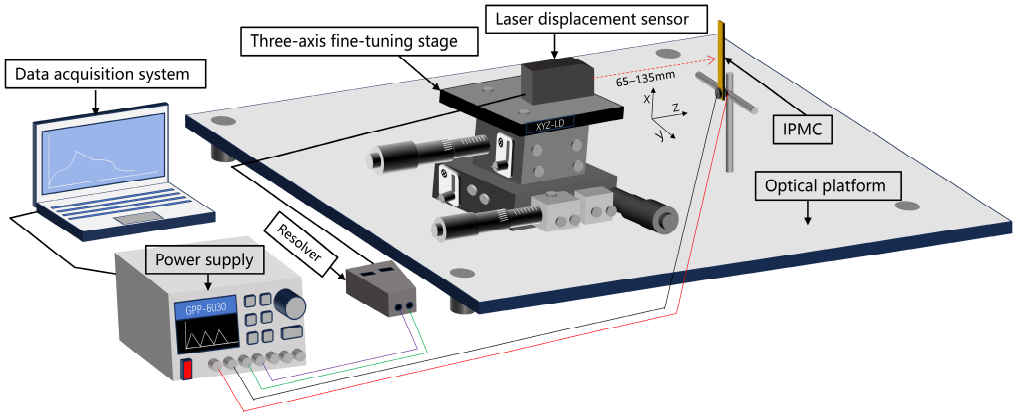

Figure 3. Electrically excited response-driven test setup for measuring the drive performance of the Cu-IPMC.

The size of the Cu-IPMC sample was 25 mm × 5 mm, and the sample was fixed to test the drive performance. The LabVIEW 2018 (Laboratory Virtual Instrument Engineering Workbench 2018) software was used to control the programmable power supply signal applied to the test Cu-IPMC samples. The deformation displacement of the Cu-IPMC samples was tested using the laser displacement sensor. In the experiments in which the drive performance was tested, the same deformation displacement test was repeated three times for each sample, and the peak displacements of these three tests were averaged.

3. Orthogonal Experiments

To improve the driving performance of the IPMC, the influence of the magnetron sputtering process parameters on the performance was studied in a relevant manner. These parameters include the argon inlet flow rate A (sccm), magnetron sputtering pressure B (Pa), magnetron sputtering power C (W), and magnetron sputtering time D (min). Owing to the many influencing factors, an orthogonal test method was adopted, with deformation angle and electrode surface resistance as the indicators. It was used to investigate the effects of these parameters. Three levels of the four aforementioned influencing factors were considered, and orthogonal experiments were designed.

As an IPMC electrode material, conductivity is a fundamental property, and copper is second only to silver in terms of conductivity. However, there is no documented information on using copper electrodes plated on the surface of Nafion membranes by magnetron sputtering. In addition, the level selection of the four parameters, namely, the magnetron sputtering power, argon flow rate, magnetron sputtering pressure, and sputtering time, was also referred to the relevant studies on the preparation of silver and platinum–copper thin films [6,26], as well as the experimental results of the pre-experiments in the preliminaries of this paper. When analyzing the factors affecting the performance of the layer, the three levels of the argon flow rate (A) were set to 20, 30, and 40 sccm, while those of the magnetron sputtering pressure (B) were set to 0.5, 0.9, and 1.3 Pa, and those of the magnetron sputtering power (C) were set to 50, 100, and 150 W. The magnetron sputtering time (D) levels were 15, 25, and 35 min [6].

The design scheme and results of the Cu-IPMCs orthogonal experiments are listed in Table 1. The Cu-IPMCs were prepared according to the process parameters corresponding to experimental numbers 1–9, and samples were cut from each Cu-IPMC for the drive response testing. Usually, the driving voltage for samples like Pd-IPMC was 1–5 V [30,31]. Since there was no literature showing the specific driving voltage for Cu-IPMC, coupled with the fact that the deformation angle remained unchanged when the previous pre-experiments drove Cu-IPMC at a DC voltage of 1–5 V. This test used a continuous voltage

boost to drive the Cu-IPMC, on the one hand, to observe the change of the deformation angle of the samples with the increase of voltage and, on the other hand, it could explore the suitable driving voltage of the Cu-IPMC. The continuous boost started at 0 V and ramped up to 60 V with a ramp rate of 1 V/1 s and a test time of 60 s. The horizontal distance between the emitting point of the laser displacement sensor and the sample under test was 120 mm, and the laser point on the sample's surface was 10 mm from the bottom of the sample strip. In general, when the strip Cu-IPMC sample bent more than 60°, it exceeded the test range of the laser displacement sensor. Therefore, when the sample bent beyond the test range, the bending displacement could be converted to the bending angle as an indicator. As shown in Figure 4, L was the length of the sample, 25 mm, D was the deformation displacement obtained from the laser displacement sensor test, H was the height of the laser point from the bottom of the sample, 10 mm, and θ was the deformation angle.

Table 1. Orthogonal experimental design scheme and results.

EXP.	A sccm	B Pa	C W	D min	Deformation Angle °	Surface Resistance Ω/cm
1	1 (20)	1 (0.5)	3 (150)	2 (25)	16.1	34.0
2	2 (30)	1 (0.5)	1 (50)	1 (15)	30.3	17.1
3	3 (40)	1 (0.5)	2 (100)	3 (35)	8.4	83.9
4	1 (20)	2 (0.9)	2 (100)	1 (15)	34.1	3.8
5	2 (30)	2 (0.9)	3 (150)	3 (35)	90.0	2.2
6	3 (40)	2 (0.9)	1 (50)	2 (25)	17.3	31.1
7	1 (20)	3 (1.3)	1 (50)	3 (35)	30.1	17.6
8	2 (30)	3 (1.3)	2 (100)	2 (25)	10.6	44.8
9	3 (40)	3 (1.3)	3 (150)	1 (15)	25.7	25.5

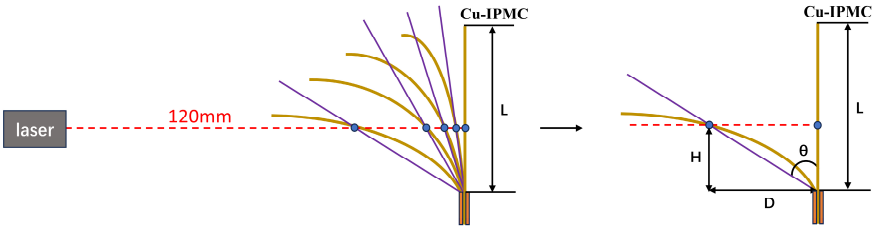

Figure 4. Schematic diagram of Cu-IPMC deformation displacement and deformation angle.

The surface resistance of the copper electrode layer significantly affects the deformation of the IPMC. To understand the surface resistance of the IPMC material, a low-resistance tester was used to test the surface resistance of the Cu-IPMC with copper electrodes. Six equally spaced points were marked on the sample at an interval of 5 mm to test the resistance between distances of 5, 10, 15, 20, and 25 mm and to determine whether the coating on the film's surface was uniform based on the change in resistance [31]. The data were measured at 1–2, 2–3, 3–4, 4–5, and 5–6, as shown in Figure 5. The surface resistance metrics in Table 2 were the total resistance from point 1 to point 6 in Figure 5.

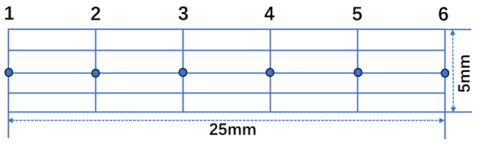

Figure 5. Surface resistance test points of the Cu-IPMC.

Table 2. Results of deformation angle range analysis.

Level	A	B	C	D
I_j	80.3	54.8	77.7	90.1
II_j	130.9	141.4	53.1	44.0
III_j	51.4	66.4	131.8	128.5
k_j	3	3	3	3
E_1	26.8	18.3	25.9	30.0
E_2	43.6	47.1	17.7	14.7
E_3	17.1	22.1	43.9	42.8
F_j	26.5	28.9	26.2	28.2
Rank	3	1	4	2

4. Results and Discussion

4.1. Effect of Sputtering Parameters on the Deformation Angle of Cu-IPMC

The parameters in Table 2 are described below: I_j, II_j, and III_j are the sum of the values of the test indicators corresponding to the "1, 2, and 3" levels in column j (j = A, B, C, and D), respectively. k_j is the number of occurrences of the same level in the jth (j = A, B, C, and D) column and is equal to the number of trials (n) divided by the number of levels in the jth column; in this case 9/3 = 3. $E_1 = I_j/k_j$, $E_2 = II_j/k_j$, and $E_3 = III_j/k_j$ are the average values of the test indices corresponding to the levels "1, 2, and 3" in column j (j = A, B, C, and D). F_j is the extreme deviation of the jth column (j = A, B, C, and D), equal to the maximum minus the minimum average of the test indicators corresponding to each level in the jth column. The rank ranks the four influencing factors according to the indicator.

According to the results of the deformation angle range analysis in Table 2, the variation of the influence of different factors on the deformation angle was obtained. The results showed that the values corresponding to the four factors of argon gas flow rate, sputtering pressure, sputtering power, and sputtering time were 26.5, 28.9, 26.2, and 28.2, respectively. As shown in Figure 6, the order of influence of different factors on the deformation angle of Cu-IPMC was sputtering pressure > sputtering time > argon gas flow rate > sputtering power. In other words, sputtering pressure was the factor with the most significant degree of influence.

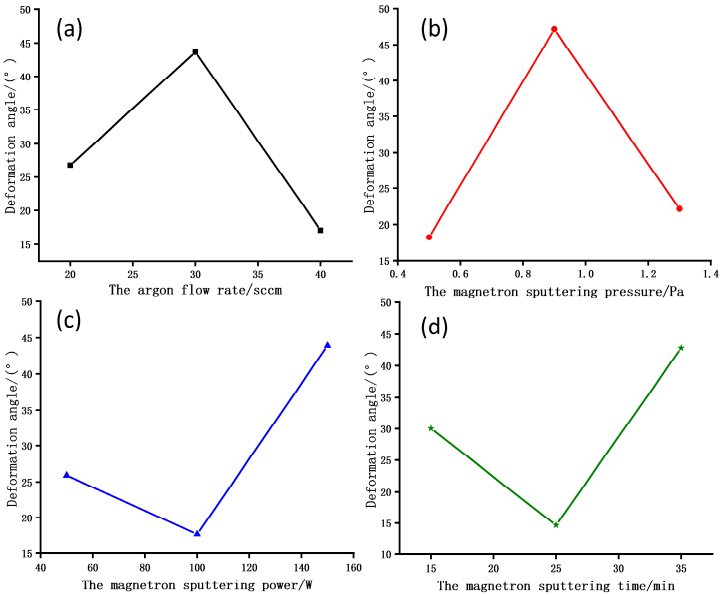

Figure 6. Effect of the (**a**) the argon flow rate, (**b**) the magnetron sputtering pressure, (**c**) the magnetron sputtering power, and (**d**) the magnetron sputtering time on sample deformation.

On comparing the mean E_1, E_2, and E_3 sizes of each column of the test index, it was concluded that: for column A, $E_2 > E_1 > E_3$, which indicates that this factor is the best at bit level 2 (30 sccm), the second best at bit level 1 (20 sccm), and the worst at bit level 3 (40 sccm). Similarly, for column B, $E_2 > E_3 > E_1$ indicates that bit level 2 is the optimum for this factor. For column C, $E_3 > E_1 > E_2$ indicates that bit level 3 is the optimum for this factor. For column D, $E_3 > E_1 > E_2$ indicates that bit level 3 is the optimum for this factor. Thus, the order of the four parameters from major to minor is $B_2D_3A_2C_3$; at this point, the corresponding sample is sample 5. Calculations to determine the optimum process parameters via the optimization experiments on the magnetron sputtering process showed that the as-prepared Cu-IPMC exhibited optimal driving performance when the magnetron sputtering pressure was 0.9 Pa, the magnetron sputtering time was 35 min, the argon flow rate was 30 sccm, and the magnetron sputtering power was 150 W. More importantly, sample 5 was prepared via magnetron sputtering within a sputtering time of 1.2 h; this duration is significantly shorter than the time required for chemical plating, which is more than 10 h [31].

A scanning electron microscope (SEM) was used to observe the surface micromorphology of five samples, as shown in Figure 7, to observe the surface morphology of Cu-IPMC materials. The magnetron sputter-plated copper metal layers exhibited no significant visible defects, but some cracks appeared, a phenomenon similar to that which was observed with platinum and silver electrodes [28,31].

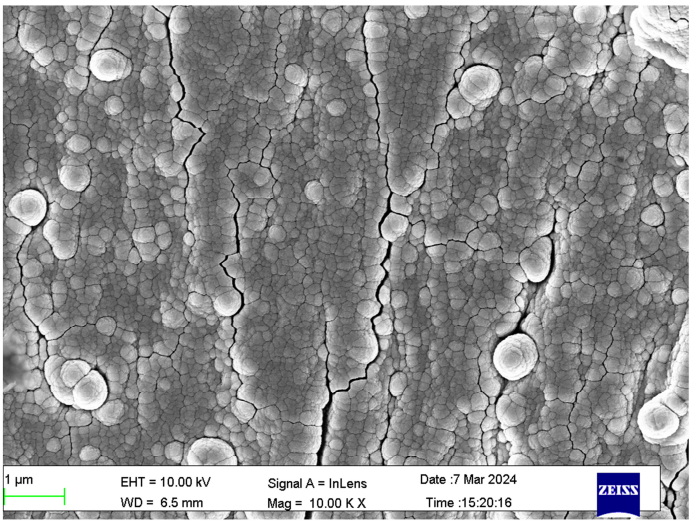

Figure 7. SEM images show the as-prepared Cu-IPMC's surface morphology (sample 5).

4.2. Effect of Sputtering Parameters on the Surface Resistance of Cu-IPMC

According to the results of the surface resistance range analysis in Table 3, the variation of the influence of different factors on surface resistance was obtained. The results showed that the values corresponding to the four factors of argon gas flow rate, sputtering pressure, sputtering power, and sputtering time were 28.4, 32.6, 23.6, and 21.2, respectively. As shown in Figure 8, the order of influence of different factors on the surface resistance of Cu-IPMC was sputtering pressure > argon gas flow rate > sputtering power > sputtering time. In other words, sputtering pressure was the factor with the most significant degree of influence. The effects of different factors on the surface resistance and the effects on the deformation angle discussed above had similar patterns of change.

Table 3. Results of surface resistance range analysis.

Level	A	B	C	D
I_j	55.4	135.0	65.7	46.3
II_j	64.1	37.1	132.5	109.8
III_j	140.5	87.8	61.7	103.8
k_j	3	3	3	3
E_1	18.5	45.0	21.9	15.4
E_2	21.6	12.4	44.2	36.6
E_3	46.8	29.3	20.6	34.6
F_j	28.4	32.6	23.6	21.2
Rank	2	1	3	4

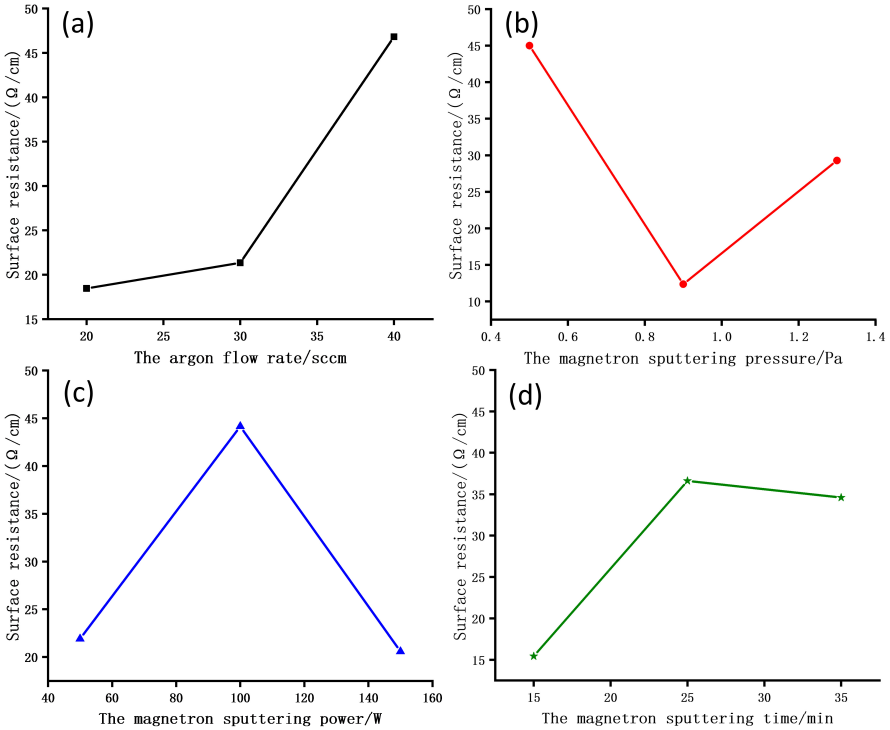

Figure 8. Effect of the (**a**) the argon flow rate, (**b**) the magnetron sputtering pressure, (**c**) the magnetron sputtering power, and (**d**) the magnetron sputtering time on sample surface resistance.

The surface resistance of Cu-IPMC in nine sets of orthogonal experiments was significantly different, indicating that the process parameters significantly affected the electrical conductivity of Cu-IPMC. As shown in Figure 8, the results indicated that Cu-IPMC with small surface resistance could be prepared by using the optimal level combination $B_2A_1C_3D_1$; the corresponding process combination parameters were a sputtering pressure of 0.9 Pa, argon flow rate of 20 sccm, sputtering power of 150 W, and sputtering time of 15 min. Compared with the optimal parameters obtained from Table 2 and Figure 6, the sputtering pressure (B) 0.9 Pa and sputtering power (C) 150 W were the same for both $B_2A_1C_3D_1$ and $B_2D_3A_2C_3$, and the difference lay in the sputtering time and argon flow rate. The sputtering pressure was the most influential factor affecting the deformation angle and surface resistance. $B_2D_3A_2C_3$ corresponded to sample 5, the resistance was relatively low, and the whole IPMC resistance was also only 2.2 Ω/cm. The resistance was 23 times lower than the traditional IPMC and 15 times lower than that of the IPMC with added multi-walled carbon nanotubes [25]. Under the comprehensive comparison, the optimal level combination $B_2D_3A_2C_3$ was finally obtained under the experimental conditions in this paper, and the optimal process parameters were a sputtering pressure of 0.9 Pa, sputtering time of 35 min, argon flow rate of 30 sccm, and sputtering power of 150 W.

The resistance test results for each segment of the experiment, sample 5, and the change in resistance with increasing distance were plotted as an image, as shown in Figure 9. From the bar graph in Figure 9, it was seen that the resistance increased as the test distance increased. This was similar to the principle of electrical resistance of metals, so the entire surface electrode could be considered a piece of intact, homogeneous copper metal, whose resistance increased linearly with increasing length for a constant cross-section. As seen from the line graph in Figure 9, there was not much difference in the resistance value of each section, reflecting the relatively homogeneous copper layer plated by magnetron sputtering.

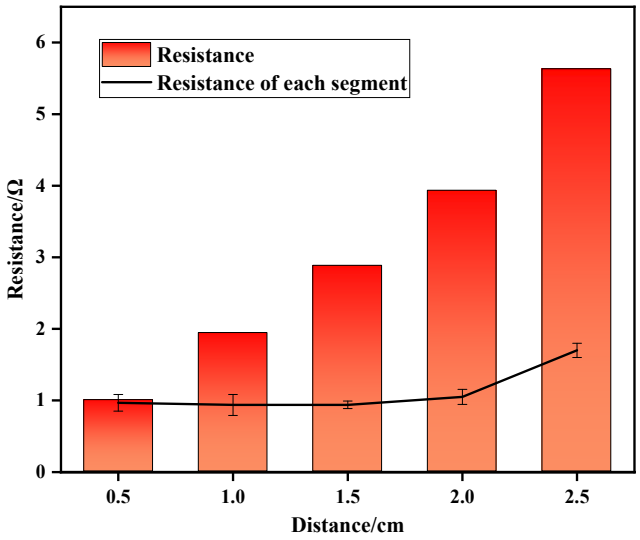

Figure 9. The surface resistance of five samples prepared by magnetron sputtering.

4.3. Copper Electrode Deposition on the Surface of the Best Sample 5

Energy-dispersive X-ray spectroscopy (EDS) was used to analyze the copper content in the IPMC; sample 5 was selected from multiple sets of Cu-IPMC samples and placed in a sealed plastic bag for one week. After the sample was placed into the sealed bag, a gas exclusion operation was performed, and the sealed bag was approximately in a vacuum state. The energy spectrum was scanned at three regional locations; the results are shown in Figure 10. Scanning the area of the Cu-IPMC surface can reflect the composition of the material elements and their average content in the area and, to a certain extent, reflect the typical material composition characteristics of the surface of the Cu-IPMC samples. Area scanning can reflect the subtle characteristics of the material components on the surface of the Cu-IPMC samples more accurately than point scanning. Therefore, areas 1, 2, and 3 were randomly selected for the scanning test.

The elemental content of the Cu-IPMC surface material was obtained by analyzing the energy spectra of the sample, as shown in Figure 10. As shown in Table 4, the mass percentages of Cu on the sample surface in the randomly selected areas 1, 2, and 3 were approximately 92.5%, 94.1%, and 94.0%, respectively, and its atomic number percentages were 76.7%, 80.6%, and 80.8%, respectively. The mass percentages of O in the selected areas 1, 2, and 3 were 1.2%, 0.5%, and 0.4%, respectively, and its atomic number percentages were 4.0%, 1.6%, and 1.4%, respectively. The surface of the Cu-IPMC samples was firmly plated with Cu, whereas O was sparse, with only approximately two out of a hundred atoms of O on average.

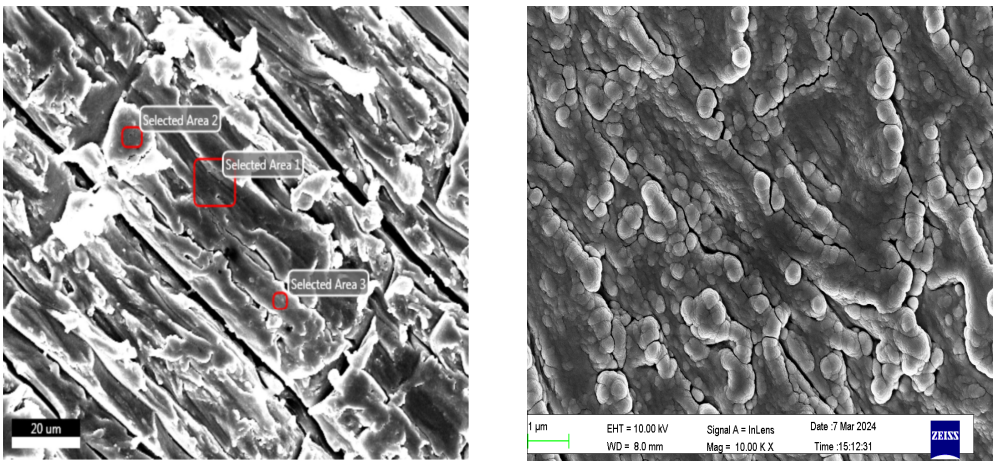

Figure 10. Energy spectra and surface morphology of the surface material of sample 5 Cu-IPMC.

Table 4. Elemental content of the surface material of the Cu-IPMC sample.

Elemental	Selected Area 1		Selected Area 2		Selected Area 3	
	Mass /%	Atomic Number /%	Mass /%	Atomic Number /%	Mass /%	Atomic Number /%
C	1.4	6.2	1.5	6.9	1.2	5.4
O	1.2	4.0	0.5	1.6	0.4	1.4
F	4.5	12.5	3.6	10.3	4.2	12.0
S	0.4	0.7	0.3	0.6	0.3	0.5
Cu	92.5	76.7	94.1	80.6	94.0	80.8

The above analysis shows that almost no Cu-oxide is present in the surface coating of the Cu-IPMC and that the Cu electrode has excellent electrical conductivity, which provides a stable electric field environment for the movement of ions within the base film.

4.4. Multi-Point Displacement Surface Fitting

In this study, a fixed DC voltage was applied to the Cu-IPMC sample, a three-axis fine-tuning platform was used to test the long-term multi-point displacement of its deformed shape, and the surface type was determined. The specific procedure is as follows: The Cu-IPMC sample was mounted onto a horizontal rod, and the DC power supply was turned on as a pair of channel outputs for the laser displacement sensor power supply such that the laser light path was parallel to the axis of the Cu-IPMC sample. The point of incidence and the center of the face shape of the Cu-IPMC sample was at a certain distance. The Cu-IPMC sample was connected to the other pair of channels of the direct current power supply using a copper piece, and the LabVIEW software was used to edit and send commands to provide the driving voltage for the Cu-IPMC. The power supply output was set to a direct current voltage of 15 V for 1800 s. The spatial coordinates of each point were measured before the end of the direct current power supply output. The measurement of the spatial coordinates (x, y, and z) of 10 points on the Cu-IPMC surface was used to fit the surface, as shown in Figure 11a.

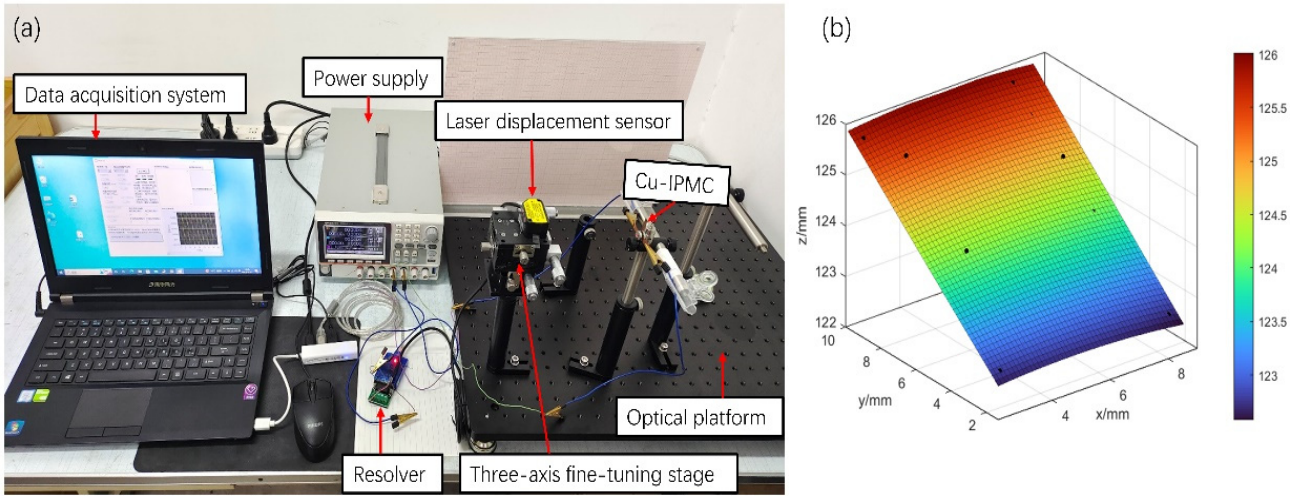

Figure 11. (**a**) Displacement test system for the Cu-IPMC and (**b**) surface fitting diagram.

The curve-fitting tool (cftool) of MATLAB R2021awas used for surface fitting based on the coordinate data, and the equations were fitted to obtain the equations of the surface formed by the long-term deformation of the Cu-IPMC.

$$z = -0.0107x^2 + 0.0003y^2 + 0.0019xy + 0.0973x + 0.3696 + 122.03 \quad (1)$$

The invariants I_1, I_2, I_3, I_4 were computed with the semivariants K_1 and K_2.

The correlation coefficient $R^2 = 0.9982 > 0.99$ was fitted, and $I_3 = 0$ and $I_4 > 0$ were obtained; the surface represented by this equation is a hyperbolic paraboloid, as shown in Figure 11b.

5. Conclusions

In this study, four influencing factors were set using theoretical calculations and orthogonal experiments, and the L_9 (3^4) orthogonal table was selected to design experiments for optimizing the parameters of the magnetron sputtering preparation process for the Cu-IPMC and for improving the stability of the driving performance.

The experimental results showed that the magnetron sputtering parameters affected the magnitude of the Cu-IPMC deformation angle in the following order: magnetron sputtering pressure, magnetron sputtering time, argon flow rate, and magnetron sputtering power. The magnetron sputtering parameters affected the magnitude of the Cu-IPMC surface resistance in the following order: magnetron sputtering pressure, argon flow rate, magnetron sputtering power, and magnetron sputtering time. For both deformation angle and surface resistance, sputtering pressure was the factor that most affected them. A comprehensive analysis of the influence of process parameters on the indexes was conducted, and the optimal level combination $B_2D_3A_2C_3$ was obtained. The process parameters were a sputtering pressure of 0.9 Pa, sputtering time of 35 min, argon flow rate of 30 sccm, and sputtering power of 150 W.

Compared with chemical plating, the Cu-IPMC sample prepared via magnetron sputtering shortened the fabrication cycle time from more than 10 h to 1.2 h; surface resistance was 2–3 Ω/cm, more than 23 times smaller than the resistance of chemical plating. Moreover, it can be used over a wider range of driving voltages and can help avoid the failure problem caused by excessive voltages, to a certain extent.

The deformation angle of the Cu-IPMC under continuous boosting was analyzed, and single-point and multi-point deformation displacement tests at different direct current voltages were conducted. Surface fitting of the long-term deformation of the Cu-IPMC was performed using the optimization software, and the result was a hyperbolic paraboloid.

However, the surface of Cu-IPMC can also develop some cracks, and oxidation may occur over time if exposed to humid air. In the next step, we will add a protective layer to

the copper electrode surface to address the lifespan issue. Additionally, we can refer to the method in [23], where the base membrane is soaked in a copper sulfate solution in advance to reduce bending cracks and increase lifespan.

Author Contributions: H.L. Formal analysis, Data curation, Writing—Original draft, Writing—Review & Editing. Z.W.: Conceptualization, Methodology, Writing—Review & Editing, Funding acquisition. J.L. (Jinping Li): Data Curation, Writing—Original Draft. C.W.: Visualization, Data curation. M.G.: Writing—Review & Editing. H.Z.: Project administration. J.L. (Jing Li): Investigation. C.Z.: Visualization. All authors have read and agreed to the published version of the manuscript.

Funding: This research was funded by the National Key Research and Development Program of China grant number 2023YFB4204301. And The APC was funded by the National Key Research and Development Program of China.

Data Availability Statement: The data presented in this study are available on request from the corresponding author due to privacy.

Conflicts of Interest: The authors declare no conflicts of interest.

References

1. Yang, L.; Wang, H.; Zhang, D.; Yang, Y.; Leng, D. Large deformation, high energy density dielectric elastomer actuators: Principles, factors, optimization, applications, and prospects. *Chem. Eng. J.* **2024**, *489*, 151402. [CrossRef]
2. Nabae, H.; Kubo, K.; Shishikura, K.; Horiuchi, T.; Asaka, K.; Endo, G.; Suzumori, K. Design and Fabrication of 3D Papercraft IPMC Robots. In Proceedings of the 2022 IEEE 5th International Conference on Soft Robotics (RoboSoft), Edinburgh, UK, 4–8 April 2022; pp. 95–102. [CrossRef]
3. Li, J.; Tian, A.; Sun, Y.; Feng, B.; Wang, H.; Zhang, X. The Development of a Venus Flytrap Inspired Soft Robot Driven by IPMC. *J. Bionic Eng.* **2023**, *20*, 406–415. [CrossRef]
4. Arnold, A.; Su, J.; Sabolsky, E.M. Nafion-Pt IPMC electroactive behavior changes in response to environmental nonequilibrium conditions. *Smart Mater. Struct.* **2023**, *32*, 055014. [CrossRef]
5. Lu, C.; Zhang, X. Ionic Polymer–Metal Composites: From Material Engineering to Flexible Applications. *Acc. Chem. Res.* **2024**, *57*, 131–139. [CrossRef] [PubMed]
6. Fu, R.; Yang, Y.; Lu, C.; Ming, Y.; Zhao, X.; Hu, Y.; Zhao, L.; Hao, J.; Chen, W. Large-Scale Fabrication of High-Performance Ionic Polymer–Metal Composite Flexible Sensors by in Situ Plasma Etching and Magnetron Sputtering. *ACS Omega* **2018**, *3*, 9146–9154. [CrossRef]
7. Ekbatani, R.Z.; Shao, K.; Khawwaf, J.; Wang, H.; Zheng, J.; Chen, X.; Nikzad, M. Control of an IPMC Soft Actuator Using Adaptive Full-Order Recursive Terminal Sliding Mode. *Actuators* **2021**, *10*, 33. [CrossRef]
8. Chang, X.L.; Chee, P.S.; Lim, E.H. Ionic Polymer Actuator With Crenellated Structures for MEMs Application. In Proceedings of the 2020 IEEE International Conference on Semiconductor Electronics (ICSE), Kuala Lumpur, Malaysia, 28–29 July 2020; pp. 160–163. [CrossRef]
9. Motreuil Ragot, P.; Hunt, A.; Sacco, L.N.; Sarro, P.M.; Mastrangeli, M. Manufacturing thin ionic polymer metal composite for sensing at the microscale. *Smart Mater. Struct.* **2023**, *32*, 035006. [CrossRef]
10. Boldini, A.; Bardella, L.; Porfiri, M. On Structural Theories for Ionic Polymer Metal Composites: Balancing Between Accuracy and Simplicity. *J. Elast.* **2020**, *141*, 227–272. [CrossRef]
11. Nasrollah, A.; Soleimanimehr, H.; Bafandeh Haghighi, S. IPMC-based actuators: An approach for measuring a linear form of its static equation. *Heliyon* **2024**, *10*, e24687. [CrossRef]
12. Wang, G.; Sun, Y.; Ji, A.; Yin, G.; Ge, H.; Liu, X.; Tong, X.; Yu, M. Review on the Research Progress and Application of IPMC Sensors. *J. Bionic Eng.* **2024**, *21*, 2687–2716. [CrossRef]
13. Shen, Q.; Palmre, V.; Stalbaum, T.; Kim, K.J. A comprehensive physics-based model encompassing variable surface resistance and underlying physics of ionic polymer–metal composite actuators. *J. Appl. Phys.* **2015**, *118*, 124904. [CrossRef]
14. Pugal, D.; Jung, K.; Aabloo, A.; Kim, K.J. Ionic polymer–metal composite mechanoelectrical transduction: Review and perspectives. *Polym. Int.* **2010**, *59*, 279–289. [CrossRef]
15. Tsugawa, M.A.; Palmre, V.; Carrico, J.D.; Kim, K.J.; Leang, K.K. Slender tube-shaped and square rod-shaped IPMC actuators with integrated sensing for soft mechatronics. *Meccanica* **2015**, *50*, 2781–2795. [CrossRef]
16. Bernat, J.; Kolota, J. Adaptive observer-based control for an IPMC actuator under varying humidity conditions. *Smart Mater. Struct.* **2018**, *27*, 055004. [CrossRef]
17. Shahinpoor, M.; Kim, K.J. Ionic polymer–metal composites: I. *Fundam. Smart Mater Struct.* **2001**, *10*, 819–833. [CrossRef]
18. Lee, J.W.; Kim, J.H.; Chun, Y.S.; Yoo, Y.T.; Hong, S.M. The performance of Nafion-based IPMC actuators containing polypyrrole/alumina composite fillers. *Macromol. Res.* **2009**, *17*, 1032–1038. [CrossRef]
19. Park, I.S.; Kim, S.M.; Pugal, D.; Huang, L.; Tam-Chang, S.W.; Kim, K.J. Visualization of the cation migration in ionic polymer–metal composite under an electric field. *Appl. Phys. Lett.* **2010**, *96*, 043301. [CrossRef]

20. Jo, C.; Pugal, D.; Oh, I.K.; Kim, K.J.; Asaka, K. Recent advances in ionic polymer–metal composite actuators and their modeling and applications. *Prog. Polym. Sci.* **2013**, *38*, 1037–1066. [CrossRef]
21. Yang, L.; Wang, H. High-performance electrically responsive artificial muscle materials for soft robot actuation. *Acta Biomater.* **2024**, *185*, 24–40. [CrossRef]
22. Wang, H.; Yang, L.; Yang, Y.; Zhang, D.; Tian, A. Highly flexible, large-deformation ionic polymer metal composites for artificial muscles: Fabrication, properties, applications, and prospects. *Chem. Eng. J.* **2023**, *469*, 143976. [CrossRef]
23. Naji, L.; Chudek, J.A.; Abel, E.W.; Baker, R.T. Electromechanical behaviour of Nafion-based soft actuators. *J. Mater. Chem. B* **2013**, *1*, 2502. [CrossRef] [PubMed]
24. Shahinpoor, M.; Kim, K.J. The effect of surface-electrode resistance on the performance of ionic polymer–metal composite (IPMC) artificial muscles. *Smart Mater. Struct* **2000**, *9*, 543–551. [CrossRef]
25. Hao, L.N.; Chen, Y.; Zhao, Y.S. Research on enhanced performance of ionic polymer metal composite by multiwalled carbon nanotubes. *Mater. Res. Innov.* **2015**, *19* (Suppl. S1), S477–S481. [CrossRef]
26. Chung, C.K.; Fung, P.K.; Hong, Y.Z.; Ju, M.S.; Lin, C.C.K.; Wu, T.C. A novel fabrication of ionic polymer–metal composites (IPMC) actuator with silver nano-powders. *Sens. Actuators B Chem.* **2006**, *117*, 367–375. [CrossRef]
27. Kim, S.M.; Kim, K.J. Palladium buffer-layered high performance ionic polymer–metal composites. *Smart Mater. Struct.* **2008**, *17*, 035011. [CrossRef]
28. He, Q.; Yin, G.; Vokoun, D.; Shen, Q.; Lu, J.; Liu, X.; Xu, X.; Yu, M.; Dai, Z. Review on Improvement, Modeling, and Application of Ionic Polymer Metal Composite Artificial Muscle. *J. Bionic Eng.* **2022**, *19*, 279–298. [CrossRef]
29. Kelly, P.J.; Arnell, R.D. Magnetron sputtering: A review of recent developments and applications. *Vacuum* **2000**, *56*, 159–172. [CrossRef]
30. Bian, C.; Zhu, Z.; Bai, W.; Chen, H. Highly efficient structure design of bending stacking actuators based on IPMC with large output force. *Smart Mater. Struct.* **2021**, *30*, 075033. [CrossRef]
31. Yang, L.; Zhang, D.; Zhang, X.; Tian, A. Fabrication and Actuation of Cu-Ionic Polymer Metal Composite. *Polymers* **2020**, *12*, 460. [CrossRef]